6-1-2023

Computational Analysis Investigation of a Piezoelectrically Actuated Micropump for Air Sniffing Applications

Yameema Babu Lopez
University of Windsor

Computational Analysis Investigation of a Piezoelectrically Actuated Micropump for Air Sniffing Applications

by

Yameema Babu Lopez

A Thesis

Submitted to the Faculty of Graduate Studies
through the Department of Electrical and Computer Engineering
in Partial Fulfillment of the Requirements for
the Degree of Master of Applied Science
at the University of Windsor

Windsor, Ontario, Canada

2023

Computational Analysis Investigation of a Piezoelectrically Actuated Micropump for Air Sniffing Applications

by

Yameema Babu Lopez

APPROVED BY:

_____
A. Azab
Department of Mechanical, Automotive and Materials Engineering

_____
E. Abdel- Raheem
Department of Electrical and Computer Engineering

_____
J. Ahamed, Co-Advisor
Department of Mechanical, Automotive and Materials Engineering

_____
A. Emadi, Co-Advisor
Departmental of Electrical and Computer Engineering

April 19, 2023

DECLARATION OF CO-AUTHORSHIP

I. Co-authorship

I hereby declare that thesis incorporate the material that is a result of joint research, as follows:

Chapter 3 and 4 of the thesis is authored by Yameema Babu Lopez under the supervision of Professor Arezoo Emadi and Professor Jalal Ahamed. In all cases, the key ideas, primary contributions, experimental designs, data analysis, interpretation, and writing were performed by the author, and the contribution of the co-author was primarily through the feedback on refinement of ideas and editing of manuscript.

I am aware of the University of Windsor Senate policy on authorship, and I certify that I have properly acknowledged the contribution of other researchers to my thesis and have obtained written permission from each of the co-author(s) to include the above material(s) in my thesis.

I certify that, with the above qualification, this thesis, and the research to which it refers, is the product of my own work.

II. General

I declare that, to the best of knowledge, my thesis does not infringe upon anyone's copy write nor violate any proprietary writes and that any ideas, techniques, quotations, or any other material from the work of other people included in my thesis, published or otherwise, are fully acknowledged in accordance with these standard referencing practices. Furthermore, to the extent that I have included copy righted material that surfaces the bounce of fair dealing within the meaning of Canada Copyright Act, I certify that I

have obtained a written permission from the copy right owner(s) to include such material in my thesis.

I declare that this is a true copy of my thesis, including any final revisions, as approved by my thesis committee and graduate studies office, and that this thesis has not been submitted for a higher degree to any other University or institution.

ABSTRACT

Micro-Electro-Mechanical Systems (MEMS) refers to a technology which uses microfabrication technology to fabricate miniaturized devices and systems. MEMS based technologies have paved the way for miniaturization and manufacturing of devices with applications ranging from biological to fluid engineering. This interdisciplinary nature of MEMS has given rise to an emerging field called microfluidics which studies devices that pump, control and sense small volumes of fluids. This work aims to investigate a piezoelectric micropump that can mimic mammalian olfaction for e-nose applications. A comprehensive literature review was conducted on all the available micropumps. A piezoelectric micropump was chosen as the candidate for this work based upon the literature review. The physics behind the micropump is studied and the critical parameters are analyzed. A computational model of the piezoelectric micropump is investigated using COMSOL Multiphysics platform and the effects of the critical parameters are analyzed. The critical parameters which include effects of piezoelectric layer, pump chamber, nozzle-diffuser elements and membrane are investigated and analyzed.

DEDICATION

To all to those who I met along the way

ACKNOWLEDGEMENTS

Firstly, I would like to express my thankfulness to my advisors Dr. Arezoo Emadi and Dr. Jalal Ahamed for their valuable advice and constant encouragement in my project, which helped me to come out successfully.

I am also thankful to my friends Gnanesh Nagesh, Mukesh Arvind Raju and my e-MINDS teammates for the help they rendered during the tough times of the project. I would also like to thank my family and friends for their support and love.

Finally, I thank THE ALMIGHTY for all the blessings showered upon me.

TABLE OF CONTENTS

DECLARATION OF CO-AUTHORSHIP iii

ABSTRACT v

DEDICATION vi

ACKNOWLEDGEMENTS vii

LIST OF TABLES x

LIST OF FIGURES xi

CHAPTER 1. Introduction 1

1.1. Motivation 1

1.2. Thesis Contribution 2

1.3. Thesis Outline 3

CHAPTER 2. MEMS-based Micropumps 4

2.1. Mechanical Micropumps 4

2.1.1. Electrostatic Micropumps 5

2.1.2. Piezoelectric Micropumps 7

2.1.3. Thermopnuematic Micropumps 8

2.1.4. Shape memory alloy (S.M.A.) Micropumps 9

2.1.5. Ion conductive polymer film (ICPF) Micropumps 10

2.1.6. Phase change type Micropumps 11

2.2. Non-Mechanical Micropumps 12

2.2.1. Electrowetting (E.W.) Micropumps 12

2.2.2. Bubble type Micropumps 13

2.2.3. Electrochemical Micropumps 14

2.2.4. Evaporation Micropumps 14

2.3. Conclusion 15

CHAPTER 3. Piezoelectric Valveless Micropump 16

3.1. Introduction 16

3.2. Structure of Piezoelectric Valveless Micropump 16

3.2.1. Design of Piezoelectric Actuator 16

3.2.2. Design of Functional Layer 17
3.2.2.1. Nozzle/Diffuser Element 18
3.2.2.2. Pump Chamber 18
3.2.2.3. Inlet and Outlet Chambers 18
3.3. Mechanism of Operation 19
3.3. Piezoelectric Effect 21
3.3.1. Molecular Model of Piezoelectric Effect 21
3.3.2. Constitutive Equations of Piezoelectric Effect 21
3.5. Fluid Flow 24
3.5.1. Flow Regime 24
3.5.2. Navier-Stokes Equation for Fluid Flow 25
3.6. Conclusion 28

CHAPTER 4. 29

Finite Element Analyses of Piezoelectric Micropump 29
4.1. Finite Element Analyses – COMSOL 29
4.2. Boundary Conditions 29
4.3. Meshing 30
4.4. Parametric Analyses on Different Geometries 31
4.4.1. Effect of PZT layer 31
4.4.2. Effect of PDMS Membrane 35
4.4.3. Effect of Pump Chamber 37
4.4.4. Effect of Nozzle-Diffuser Elements 39
4.5. Conclusion 43

CHAPTER 5 44

Conclusion and Future Scope 44
5.1. Future Scope 45

REFERENCES/BIBLIOGRAPHY 46

VITA AUCTORIS 51

LIST OF TABLES

Table 1. Design parameters for piezoelectric actuator..... 17
Table 2. Design parameters for functional layer..... 19
Table 3. Parameters for studying the effect of PZT layer diameter..... 32
Table 4. Parameters for studying the effect of PZT layer thickness..... 35
Table 5. Parameters for studying the effect of PZT layer thickness..... 36
Table 6. Parameters for studying the effect of pump chamber thickness..... 38
Table 7. Parameters for studying the effect of nozzle-diffuser angle..... 40
Table 8. Parameters for studying the effect of nozzle-diffuser length..... 42

LIST OF FIGURES

Figure 2. 1. A schematic representation of Electrostatic Micropump 5
Figure 2. 2. A schematic representation of Piezoelectric Micropump..... 7
Figure 2. 3. A schematic representation of Thermopneumatic Micropump 8
Figure 2. 4. A schematic representation of Shape Memory Alloy Micropump..... 9
Figure 2. 5. A schematic representation of ICPF Micropump 10
Figure 2. 6. A schematic representation of Phase Change Micropump..... 11
Figure 2. 7. A schematic representation of Electrowetting Micropump..... 12
Figure 2. 8. A schematic representation of Bubble Type Micropump..... 13
Figure 2. 9. A schematic representation of Electrochemical Micropump 14
Figure 2. 10. A schematic representation of Evaporation Type Micropump..... 15

Figure 3. 1. Piezoelectric Valveless Micropump 16
Figure 3. 2 Outward deflection of the membrane in piezoelectric micropump 20
Figure 3. 3 Inward deflection of the membrane in piezoelectric micro[ump 20

Figure 4. 1 Boundary Conditions applied on the piezoelectric micropump in COMSOL Multiphysics platform..... 30
Figure 4. 2. COMSOL Simulation results showing the maximum displacement versus mesh type for a piezoelectric micropump biased at 40 V 31
Figure 4. 3. . Maximum displacement for various diameters of PZT layer of the micropump biased at 40 V, 80 V and 120V..... 33
Figure 4. 4. Maximum volume pumped for various diameters of PZT layer of the micropump biased at 40 V, 80 V and 120V..... 33
Figure 4. 5. Von Mises Stress for various PZT layer diameters biased at 40 V using COMSOL Multiphysics Platform..... 34
Figure 4. 6. Maximum displacement for various thickness of PZT layer of the micropump biased at 40 V, 80 V and 120V..... 35
Figure 4. 7. Maximum volume pumped for various thickness of PZT layer of the micropump biased at 40 V, 80 V and 120 V..... 35
Figure 4. 8. Maximum displacement for various thickness of PDMS layer of the micropump biased at 40 V 36
Figure 4. 9. Maximum volume pumped for various thickness of PDMS layer of the micropump biased at 40 V 37

Figure 4. 10. Maximum displacement for various thickness of pump chamber of the micropump biased at 40 V 38
Figure 4. 11. Maximum volume pumped for various thickness of pump chamber of the micropump biased at 40 V 39
Figure 4. 12. Schematic diagram of a Conical Nozzle- Diffuser..... 40
Figure 4. 13. Maximum displacement for various nozzle-diffuser angles biased at 40 V 41
Figure 4. 14. Maximum volume pumped for various nozzle-diffuser angles biased at 40 V 41
Figure 4. 15. Maximum displacement for various nozzle-diffuser lengths biased at 40 V 42
Figure 4. 16. Maximum volume pumped for various nozzle-diffuser lengths biased at 40 V..... 43

CHAPTER 1.
Introduction

1.1. Motivation

The greenhouse sector is a fast-growing area in Canadian horticulture. The Canadian greenhouse sector has experienced a massive upward trend in its growth. The sector grows common vegetables like cucumber, tomatoes, peppers, eggplants and so on. The sector has rapidly expanded contributing to 1.95 billion to Canadian economy [1].

With the expansion of industry in the economy, it also faces several challenges. One of the major challenges faced by the greenhouse sector is pest management issue. In order to eradicate pests, pesticides and other bioagents are used. However, the diagnosis happens at a later state. The plant-pest diagnosis can be done at earlier stages if the volatile organic compounds released by the plants are identified. Several traditional methods such as gas-chromatography mass spectroscopy methods are used for the identification of volatile organic compounds.

Deviating from the above conventional techniques, this research proposes to adopt a MEMS based micropump which is used in an e-nose system for controlling pests by identifying the volatile organic compounds released by the plants. The micropump mimics mammalian olfaction that pumps a controlled volume of air in. The micropump takes in a certain volume of the air from the surrounding environment and pumps it to the sensing chamber that detects the volatile organic compounds released by the plants [2]. This will serve as a cost-effective tool that is capable of early diagnosis of the plants at a fast pace, compared to the bulky expensive lab techniques [2]. Also, the mentioned detection technique is less time consuming compared to the conventional techniques [2].

During the past years, many different types of micropumps have been developed. Actuation principles like electromagnetic, piezoelectric, osmotic, magnetohydrodynamic, thermopneumatic, electrostatic or electro hydrodynamic and more have been investigated. For gaseous pumping, the displacement of the gas, followed by transportation through valves, is required [3]. Some of the actuation principles mentioned above cannot be applied for pumping air (osmotic, electrohydrodynamic, magneto-

hydrodynamic), as these principles need the properties of a liquid for actuation [3]. The stroke of electrostatic actuation is too small to compress gas to a sufficient compression ratio [3]. Thermopneumatic actuation exerts higher strokes, but huge energy consumption and low pump frequencies are associated drawbacks [3]. For these reasons, especially piezoelectrically driven micropumps seem suitable as a air sniffer which is used in e-nose for controlling pest by identifying the volatile organic compounds released by the plants [4].

This thesis aims to investigate a piezoelectric micropump as a sniffer operating on ambient conditions which is proposed to be integrated with the sensing chamber of the e-nose system. The major challenge of the project is controlling the volume of the air sample which can be controlled using the driving voltage on the piezoelectric disc [5]. The gas flow of the system is solved using compressible Naiver-Stokes equation and a three-dimensional system is developed using COMSOL Multiphysics platform. Parametric sweeps are performed to ensure the working of the micropump at ambient operating conditions. The materials are chosen for the model by conducting a comprehensive literature review which makes the device more cost-effective.

1.2. Thesis Contribution

In this thesis, a piezoelectrically actuated micropump is investigated and analyzed which is capable for sniffing applications. The major objective of this thesis is to investigate a micropump which is capable of mimicking mammalian olfaction. In order to design such a micropump, a comprehensive review is conducted on available micropumps. From this review, a comprehensive approach is taken to study the principle of operation, the critical design parameters and the related governing equations.

The effect of piezoelectricity is studied along with the compressible laminar flow studies. An analytical modelling has been proposed for the proposed micropump structure. From this analytical modelling the displacement and the volume of the air pumped is calculated. Incorporating these physics equations in the finite element analysis modelling software COMSOL a geometry is designed and critical parameters like radii, thickness, length and angles of the proposed design is analyzed and studied.

1.3. Thesis Outline

Chapter 2, various micropumps are reviewed based on their principle of operation, advantages and disadvantages.

Chapter 3 provides an insight into piezoelectric micropumps with its review, design, operating principle, design parameters and governing equations.

Chapter 4, focuses on computational analysis using finite element analysis is presented. A three-dimensional finite element model of piezoelectric micropump was built using COMSOL Multiphysics 5.5 software is presented. The effect of radius on the total surface displacement, effect of different voltages on the total surface displacement, velocity vs pressure analysis and eigen frequency analysis are discussed.

Finally, conclusion and the summary of the conducted research in this work are provided in **Chapter 5** in addition to the possible future works.

CHAPTER 2.
MEMS-based Micropumps

Micro-Electro-Mechanical Systems (MEMS) refers to a technology which uses microfabrication technology to fabricate miniaturized devices and systems [6]. MEMS based technologies have paved the way for miniaturization and manufacturing of devices with applications ranging from biological to fluid engineering. This interdisciplinary nature of MEMS has given rise to an emerging field called microfluidics [6].

Microfluidics deals with the design and development of miniaturized devices that can pump, sense, monitor, and control small volumes of fluid [1]. In the past few years, there has been a growing interest in the development of microfluidic systems for various applications, including biological and chemical analysis, lab-on-chip diagnostics and drug delivery [6]. Micropump is an integral element in such microfluidic systems as it is essential for micro liquid handling [6].

Micropumps are miniaturized devices that are capable of handling flow rates in the range of microliter per minute to milliliter per minute [6]. In recent years, many micropumps based on various actuation schemes have been proposed to cater to the growing needs of human in sectors like automotive, aerospace, medicine and so on [6]. Based on the actuation energy to drive the fluid flow, micropumps can be divided into two categories: Mechanical and Non-Mechanical Micropumps [1]. This chapter investigates the collective actuation schemes, structures, principles of operation along with merits and demerits associated with each of the micropumps.

2.1. Mechanical Micropumps

Mechanical micropumps requires a physical actuator or a mechanism to perform pumping action [6]. Mechanical micropumps have moving parts like pumping diaphragm or check valves [6]. Some of the actuation schemes used by mechanical micropumps include electrostatic [7-10], piezoelectric [11-18], thermopnuematic [19-21], shape memory alloy [22-25], Ion Conductive Polymer Film (ICPF) [26-27], and phase change type [27-29]. Mechanical micropumps commonly consist of a pump chamber which is

affixed by a flexible diaphragm [6]. Fluid flow is driven by, over and under pressure created in the chamber [6]. Under pressure causes an inflow of fluid, whereas overpressure causes an outflow of the fluid. Categorization of mechanical micropumps based on the actuation schemes is assessed in further sections.

2.1.1. Electrostatic Micropumps

Electrostatic micropumps consist of two electrodes with an electrode spacing that is attached to a diaphragm, a pump chamber, microchannel, inlet, and outlet [7], as shown in Figure 1.1.

Electrostatic actuation is achieved by Coulomb's attraction force between oppositely charged plates. The Coulomb's attraction force generated between the plates, when a voltage is applied can be expressed as [8],

$$F = \frac{dW}{dx} = \frac{1}{2}\frac{(\varepsilon_0 \varepsilon_r A V^2)}{x^2} \tag{1.1}$$

where F is the electrostatic actuation force, W the energy stored, ε (= $\varepsilon_0\varepsilon_r$) the dielectric constant, A is the electrode area, V the voltage applied, and x is the electrode spacing [8].

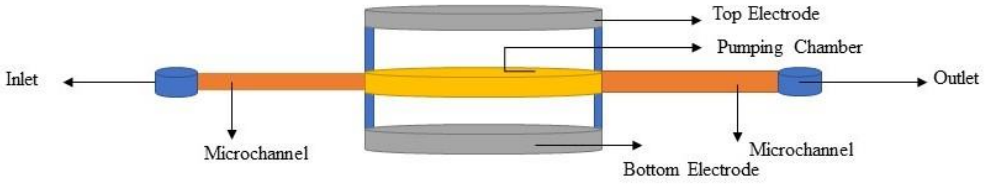

Figure 2. 1. A schematic representation of Electrostatic Micropump (not to scale)

In an electrostatic micropump, the application of appropriate voltage on the oppositely charged plates on both sides causes the membrane of the electrostatic micropump to deflect in either direction. As a result of the deflection, pressure induced by the membrane causes the fluid in the chamber to flow in the microchannels [9]. If the applied voltage is disconnected, the deflected membrane returns to its initial position. The chamber volume inside the micropump varies by alternate switching of the applied voltage [10].

Different fabrication schemes are employed for electrostatic micropumps. The collective fabrication schemes include bulk micromachining, silicon micromachining and plastic injection molding with post-processing [7-11]. Bulk micromachined pumps offer high flow rates compared to silicon micromachined pumps because the former etches a thick layer of silicon providing deeper channels and structural rigidity [7]. The latter still have advantages due to batch fabrication [10]. Plastic injection molded micropumps are more accessible to fabrication and offer excellent reliability because of simpler design, corrosion resistance and low friction [10].

Experimental verification includes the use of laser vibrometer to study the membrane characteristics, leakage estimation by applying pressure to the valves to study the flow characteristics, gravimetric detection of mass per minute of a long capillary tube on the scale to obtain flow rates and pneumatic actuation to detect the presence of bubbles [7-11].

The advantages of electrostatic micropumps are low power consumption, fast response time and stroke volume, which is easily controlled by the applied voltage [7-10]. The major disadvantage is the smaller displacement of the membrane despite the application of a higher actuation voltage.

The major applications include implantable medicine dosage control, fuel injection, microscopic fluid or gas sampling, fluid transport or fluid mixing, portable and wearable applications, and drug delivery applications [7-10].

2.1.2. Piezoelectric Micropumps

Piezoelectric micropump consists of a piezoelectric disc that is attached to a diaphragm, a pump chamber, microchannels, inlet, and outlet, as shown in Figure 1.2 [10]. Piezoelectric actuation was the first actuation principle used in micropumps [11]. The deformation of the piezoelectric materials is achieved by actuation [12]. On account of the piezoelectric effect, a strain is induced by the electric field, which causes an oscillatory motion, propelling the fluid flow [13].

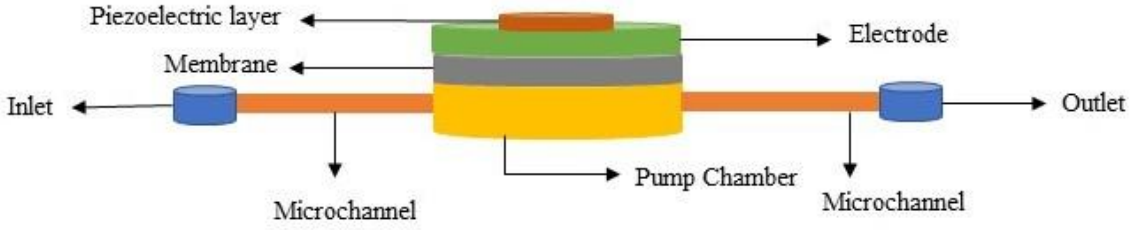

Figure 2. 2. A schematic representation of Piezoelectric Micropump (not to scale)

The voltage is applied on top of the piezolectric layer and the electrode is chosen as the ground. When an electric field is applied to the top of the piezoelectric disc, it induces a deformation on the membrane. The applied voltage across the piezoelectric membrane leads to an actuating force on the membrane [14]. Due to the elastic property of the membrane, it behaves like a spring creating an oscillatory motion [14]. Oscillatory motion creates an outward (supply mode) and inward deflection (pump model). In the supply model, the outward deflection of the membrane causes an increase in the pump chamber volume, which decreases the pressure inside the pump chamber. In the pump mode, the inward deflection of the membrane causes an increase in the pump chamber volume, which decreases the pressure inside the pump chamber. This actuation mechanism drives the fluid from the inlet to the outlet.

The employed fabrication schemes are silicon on insulator, wet etching, deep reactive ion etching and anodic bonding. Fabricated models are typically examined for membrane

deflection using laser vibrometer, flow rate analysis using flow sensor and pressure-flow characteristics using a pressure sensor [11-18].

Typical features consist of comparatively high stroke volume, a high actuation force and a fast-mechanical response [11-18]. The moderately high actuation voltage and the mounting procedure of the piezoelectric disk can be regarded as drawbacks [11-18]. Applications are limited not only in the area of drug delivery, transdermal insulin delivery but also in sphincter prosthesis and point of care systems [11-18].

2.1.3. Thermopnuematic Micropumps

The thermopunematic micropump, as shown in Figure 1.3, consists of an actuator, microchannels, valves, inlet, and outlet [19]. The actuator includes a cavity filled with air, a pump membrane, and a built-in resistive heater. Thermopneumatic actuation involves thermally induced volume change of fluids enclosed in a cavity with at least one compliant wall [19]. The application of an electric voltage to the heater causes a temperature rise of air inside the chamber, followed by a downward deflection of the pump membrane due to the induced pressure. The pressure difference induced by the voltage forces the opening and closing of the inlet and outlet valves, respectively.

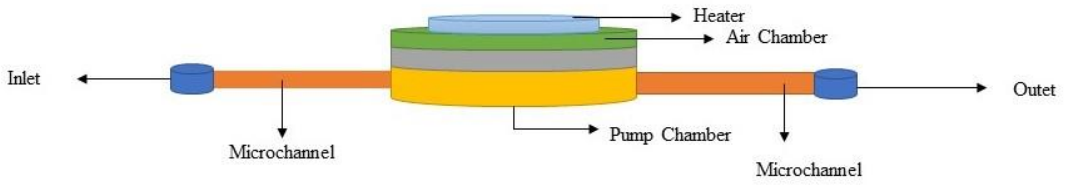

Figure 2. 3. A schematic representation of Thermopneumatic Micropump (not to scale)

The commonly employed fabrication scheme is spin-coating [19-21]. Fabricated models are usually employed for flow rate characteristics. Also, the fabricated models were sensitive towards the bubbles in the pump chamber [19-21].

Substantial induced pressure and displacement of the membrane are the merits associated with these pumps but suffer from high-power consumption and slow response time. The investigated reports point applications in cryogenic systems, lab-on-chip, and drug delivery systems [19-21].

2.1.4. Shape memory alloy (S.M.A.) Micropumps

The Shape Memory Alloy (S.M.A.) micropumps comprises of shape memory alloy actuator unit, pump chamber, microchannels, inlet and outlet as shown in Figure 1.4 [22]. S.M.A. makes use of the shape memory effect in which there is reversible solid-state transformation of the material from a low temperature, easily deformable martensite to a high temperature, relatively rigid austenite [23]. The transformations associated with these pumps, there is a thermal hysteresis which is process, history, and stress dependent [22-23]. As the pump is driven by an electric drive signal, it causes a Joule heating induced phase transformation. This initiates the shape memory effect, forcing the fluid to enter the chamber. The inverse occurs when the voltage is limited to zero.

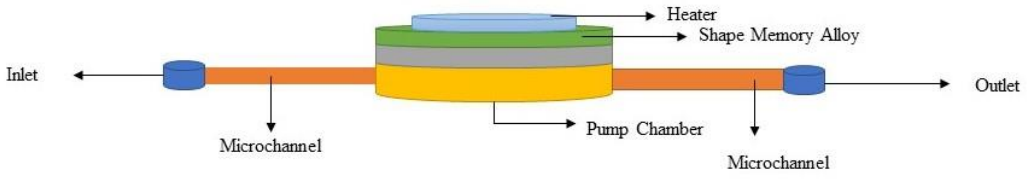

Figure 2. 4. A schematic representation of Shape Memory Alloy Micropump (not to scale)

Owing to its high actuation work density and recoverable strain, TiNi is chosen as the material for the actuator in many of the developed applications [22-2]. The flow characteristics as a function of pressure is the commonly studied output. One of the other studies include the use of a mass balance to measure the quantity of the fluid as a function of time [22-24].

High pumping yield, high working frequency and long fatigue lifetime are the advantages of such micropumps [22-24]. The disadvantages include complex behavior of the

actuating system, higher power consumption and slow response time [22-24]. The major application includes intracavity intervention [22-25].

2.1.5. Ion conductive polymer film (ICPF) Micropumps

In these micropumps, Ion Conductive Polymer Film (ICPF) is used as the servo actuator as illustrated in the Figure 1.5 [26]. The structure also includes a pump chamber, microchannels, diaphragm, ICPF is actuated through the stress gradient by ionic movement due to the electric field [26]. ICPF actuator is made from the film of perfluoro sulphonic acid polymer chemically plated with platinum on both sides of the film. It is a high polymer gel actuator that operates only in water and wet conditions [26].

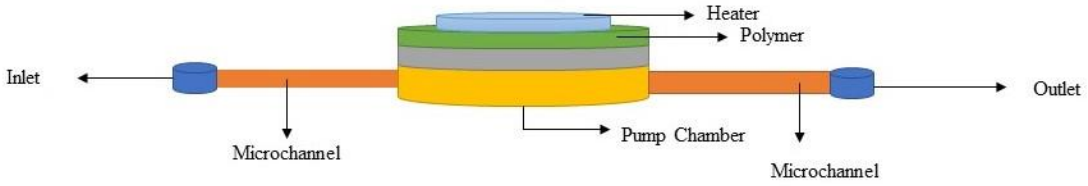

Figure 2. 5. A schematic representation of ICPF Micropump (not to scale)

By the application of the electricity, the actuator is bent on its anode side, which increases the volume in the pump chamber resulting in the inflow of the fluid [26]. By reversing the current direction, the volume inside the chamber decreases, resulting in the outflow liquid flow from the chamber to the outlet. An application of the sinusoidal voltage repeatedly pumps in and out the fluid from the pump chamber [26].

The most frequently used experimental setup requires the usage of a computer to vary the electrical voltage on the actuator, and the electrical current is measured using a galvanometer. The displacement produced by the actuator is commonly measured by a laser displacement sensor. The response characteristic and maximum displacement of the valves were studied by changing the frequency of the input voltage [27].

The advantages are low actuation voltage, faster response time and biocompatibility [26, 27]. However, the fabrication is complex. Reported applications of ICPF are in intracavity intervention, robotics, and manipulators [26, 27].

2.1.6. Phase change type Micropumps

Phase change micropumps consists of heater, working fluid chamber, diaphragm, microchannel, inlet and outlet as shown in Figure 1.6 [28]. The actuating mechanism of the phase change type micropump is based on the vaporization and condensation of the working fluid. The actuator consists of a membrane, microheater and working fluid chamber [28].

(not to scale)

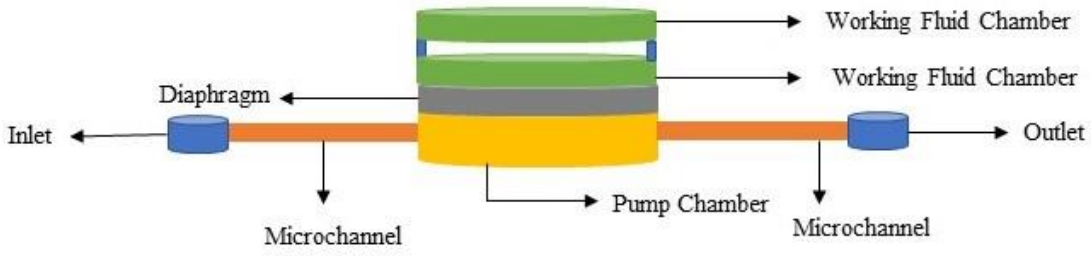

Figure 2. 6. A schematic representation of Phase Change Micropump (not to scale)

The application of input power to the microheater in the phase change type actuator heats and vaporizes the working fluid. As a result, the pressure increase in the working fluid chamber swells the membrane [25]. At the point when the power is cut off, the membrane is restored to its original state due to condensation. If an input voltage is applied to the heater, the membrane vibrates, resulting in the fluid being repeatedly sucked in and pumped out of the micropump through valves [25].

Micromachining technologies involve PECVD for the fabrication of thermal actuator, reactive ion etching for external circuits and electrochemical discharge machining for boring of feed holes [25]. The fabricated model was experimentally verified for checking valve flow characteristics by applying a static pressure difference between the inlet and the outlet. The displacement of the meniscus in the capillary tube is observed and recorded using a video microscope and a video recorder [25].

The advantages of the micropump includes the low pressure and high flow rates [26]. The disadvantages include complex structure, low efficiency, and slow reaction time [26]. The reported applications include lab-on-chip [26].

2.2. Non-Mechanical Micropumps

Non-mechanical micropumps transforms available non-mechanical energy into kinetic momentum [6]. These micropumps have no mechanical moving parts. Some of these micropumps are based on electrowetting, bubble type, electrochemical and evaporation [6]. The design and geometry are simpler compared to non-mechanical micropump. However, they have limitations such as the use of only low conductivity fluids, and the actuation mechanisms are such that they interfere with the pumping liquid [6]. The following sections investigates the common non-mechanical micropumps.

2.2.1. Electrowetting (E.W.) Micropumps

Electrowetting (E.W.) micropumps includes electrodes, pump chamber, inlet, outlet and microchannels as shown in Figure 1.7 [27]. Electrowetting is an electrically stimulated change of a material's wettability. Wettability change is achieved by the application of the electrical voltage. The structure includes electrodes, inlet, outlet, and pump chamber [27].

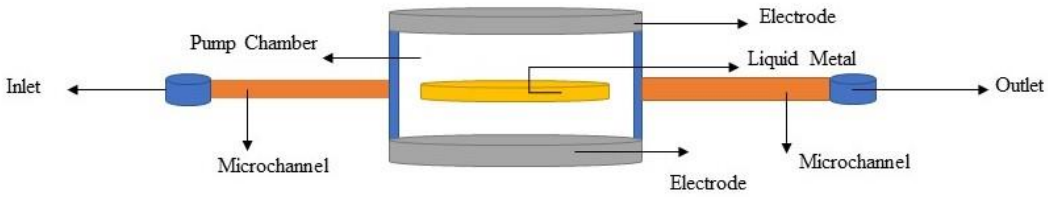

Figure 2. 7. A schematic representation of Electrowetting Micropump (not to scale)

When an electrical voltage is applied to the electrodes, a change in charge distribution occurs. This variation further gives rise to a change in the surface tension driving the inflow and outflow of the fluid. A continuous E.W. is applied to adjust the interfacial energy/ surface tension of two immiscible liquids such as liquid metal like mercury and

electrolyte. The protonation effect on the mercury surface creates a difference in the surface tension to achieve the fluid flow.

The fabrication schemes employed comprises of spin coating, photolithography, patterning, and reactive ion etching [27, 28]. The fabricated device was experimentally verified for the displacement studies using laser deflectometer, and flow characteristic studies. Low power consumption and faster speed are the merits associated with the pump. However, the pump suffers from contamination of the fluid [27, 28].

2.2.2. Bubble type Micropumps

The design of bubble type micropumps is comprised of heater, inlet, outlet chambers, pump chambers and microchannels as shown in Figure 1.8 [29]. The bubble type micropump is driven by the intermittent expansion and collapse of the bubble generated in the reservoir. With the application of applied voltage, a thermally actuated microbubble is generated within the pumping chamber. The generated bubble expands and collapses, resulting in the pumping action of the fluid.

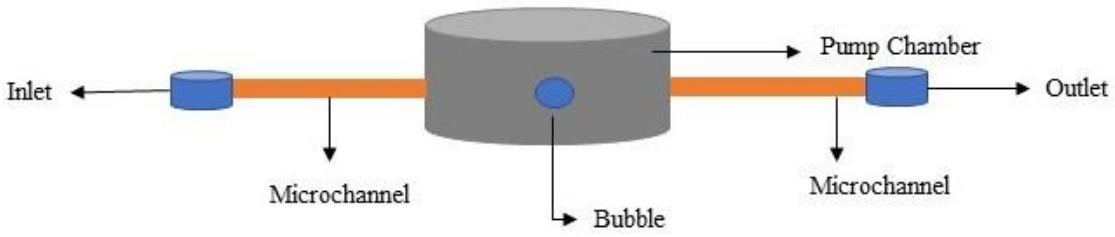

Figure 2. 8. A schematic representation of Bubble Type Micropump (not to scale)

Reported fabrication schemes include silicon on insulator, laser machining and other micromachining techniques [29, 30]. Easier integration into other microfluidic devices and controlled flow rates were the merits. The constant thermal actuation of bubbles restricts the applications associated with the device. Continuous monitoring of glucose levels in patients was one of the reported applications [30].

2.2.3. Electrochemical Micropumps

The structure of the micropump is composed of electrodes, fluid channels, pump chamber and inlet and outlet chambers as illustrated in Figure 1.9 [31]. The electrochemical pump is powered by bubbling action caused by the electrolysis of the fluid.

As a result of the voltage applied, the electrolysis takes place, creating a pressure build-up in the chamber which dispenses the fluid. The catalytic action of the electrodes ceases the formation of bubbles. The formation of the bubbles power up the working of the pump and serves as a significant driving factor [32].

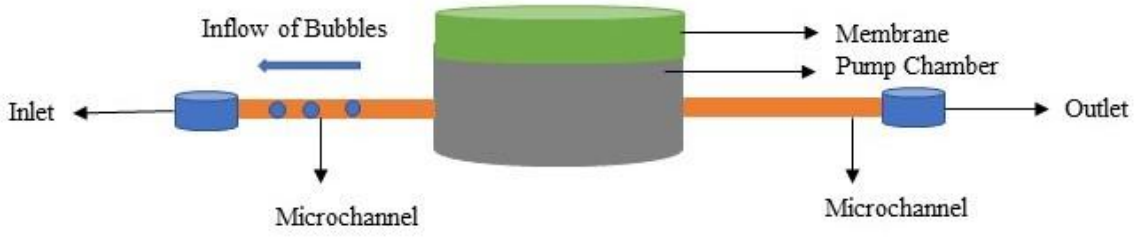

Figure 2. 9. A schematic representation of Electrochemical Micropump (not to scale)

The construction of the pump is simple and can be easily integrated with other microfluidic devices. The limitation is the collapse of the formed bubbles to create a turbulence in the pump chamber. The pump was used to power up the micro-insulin injection system and chemical stimulation of neurotransmitters [31, 32].

2.2.4. Evaporation Micropumps

Evaporation type micropumps consists of membrane, pump chamber with sorption agent, inlet and microchannel as shown in Figure 1.10 [33]. Evaporation micropumps operates by the principle in which the fluid is evaporated by controlled means through a membrane to a gas holding chamber. The vapor pressure of the gas is replaced by the capillary forces to achieve the inflow of the fluid [34].

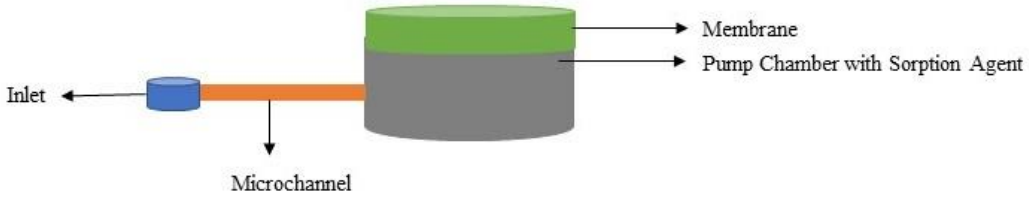

Figure 2. 10. A schematic representation of Evaporation Type Micropump (not to scale)

The inexpensive fabrication schemed pump delivers a constant flow rate and high reliability [33, 34]. The pump also does not require any external energy source, which is also an added advantage. Demerits include a lower flow rate and means of operation only in suction mode [33, 34]. Glucose monitoring in patients was one of the application areas associated with the micropump.

2.3. Conclusion

During the past years, many distinct types of micropumps have been developed. As part of the conducted investigation of various micropump for gaseous pumping, the displacement of the gas, followed by transportation through valves, is required. The investigational analysis concluded that some of the actuation principles mentioned above could not be applied for pumping air, as the principles of some of the micropumps require the properties of a liquid for actuation. For these reasons, piezoelectrically driven micropumps seem suitable as a candidate for mimicking mammalian olfaction. Hence, the focus of this thesis will be on the investigation of a piezoelectric micropump as an air sniffer to achieve controlled volume.

CHAPTER 3.

Piezoelectric Valveless Micropump

3.1. Introduction

Piezoelectric valveless micropump is one of the candidates for pumping fluids that can mimic mammalian olfaction [3]. It has received immense attention in the recent past owing to its advantages like uncomplicated design, faster response, and larger mechanical stress [12-19]. This chapter aims to discuss in detail the structure, working mechanism and physics of operation of the piezoelectric valveless micropump.

3.2. Structure of Piezoelectric Valveless Micropump

The piezoelectric valveless micropump in this work consists of a piezoelectric disk attached on top of a diaphragm which is connected to the pump chamber, inlet and outlet using flow rectifiers as shown in Figure 3.1 [13].

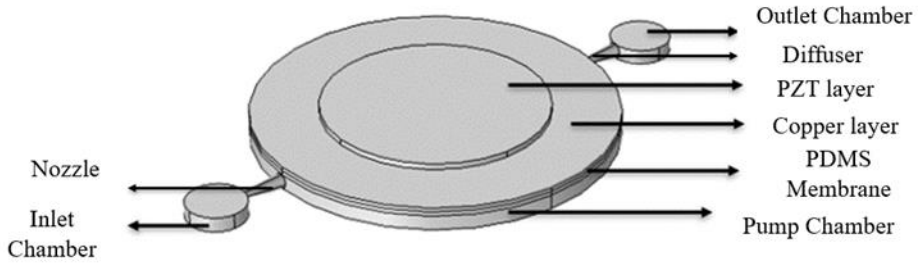

Figure 3. 1. Piezoelectric Valveless Micropump

3.2.1. Design of Piezoelectric Actuator

The piezoelectric actuator comprises of a piezoelectric layer mounted on a conductive layer [14]. The piezoelectric layer requires a material with high strain (charge) constants, permittivity, and coupling constants. Lead-Zirconate Titanate (PZT 5H) satisfies the properties required for a piezoelectric layer afore mentioned [15]. It provides larger

displacements in micrometer range even at lower voltages making it suitable for the construction of piezoelectric layer [15]. Copper (Cu) is chosen as the material for the metallic disc because of its highly-conductivity, corrosion resistance and ductility [16]. Also, copper is cheaper compared to other materials. The membrane requires a material with appreciable elasticity. Polydimethylsiloxane (PDMS) is an elastomer which is deformable, transparent, easy to mold, biocompatible and inexpensive making it an ideal material for microfluidic applications [17]. The proposed design parameters for the same are discussed in Table 3.1. The design parameters were chosen based on the work of Rohit et. al. However, deviating from their work, this model adopts DC voltage and laminar compressible flow for the functioning of the micropump.

Name	Value	Description
d	7.5[mm]	PZT layer diameter
t	0.2[mm]	PZT layer thickness
d1	12[mm]	Copper layer diameter
t1	0.14[mm]	Copper layer thickness
d2	12[mm]	PDMS diaphragm diameter
t2	0.15[mm]	PDMS diaphragm thickness
Vin	40[V]	Voltage Applied

Table 1. Design parameters for piezoelectric actuator

The diameter of the PZT layer (7.5 mm) is chosen lesser compared to the diameter of the copper layer (12 mm) as the above designed micropump offers comparatively higher displacements which is further discussed in Chapter 4. The thickness of the PZT layer (0.2 mm) and Copper layer (0.14 mm) cannot be lesser than 0.1 mm as sizes lesser than that are difficult to fabricate. The PDMS diaphragm diameter (12 mm) is selected in such a way that it encloses the pump chamber (12 mm). The maximum coercive field of a PZT layer is 8 kV/cm (160 V), more than that leads to breakdown. Hence, the voltage applied for the piezoelectric micropump is 40 V.

3.2.2. Design of Functional Layer

The functional layer (since this layer uses the working fluid air) consists of the inlet, nozzle/diffuser elements, pump chamber and outlet. The overpressure and under pressure

in the pump chamber propel the flow of the fluid. Air is the fluid medium in this work. The proposed design parameters are discussed in Table 3.2.

3.2.2.1. Nozzle/Diffuser Element

A nozzle/diffuser element is a device that accelerates/decelerates the fluid flow [17]. A nozzle is a structure with increasing cross-section whereas diffuser is a structure with decreasing cross-section. The nozzle with increasing cross-section causes the fluid flow to increase the velocity. The diffuser with decreasing cross-section decreases the velocity of the fluid flow

Nozzle/Diffuser have different geometrical shapes like planar, pyramidal and conical [35]. A conical geometry is chosen for the designed micropump due its simple geometry and ease of integration to the pump chamber. The two structures nozzle and diffuser have similar geometry since they are designed to perform opposite functions of fluid flow in the micropump and to increase efficiency. The nozzle is used at the inlet section and the diffuser is used at the outlet section of the micropump.

3.2.2.2. Pump Chamber

The bottom central section of the micropump is the pump chamber. The geometry of the pump chamber should be chosen in such a way that it could accommodate the piezoelectric actuator on top of it. The pump chamber diameter is chosen a larger value compared to the piezoelectric actuator so that various diameters of the piezoelectric actuator can be incorporated and studied using the finite element analysis tool COMSOL discussed in Chapter 4. Pressure variations induced because of the piezoelectric effect allows for the fluid flow inside the pump chamber.

3.2.2.3. Inlet and Outlet Chambers

Inlet and outlet chambers are cylindrical structures with the same dimensions. One of the boundaries of the inlet chamber is chosen as inlet for the entry of the fluid and one of the boundaries is chosen as the outlet for the exit of the fluid from the pump chamber. During the supply mode, the fluid is forced into the pump chamber from the inlet and outlet chambers. Whereas in the pump mode the fluid is discharged from the pump chamber.

Name	Value	Description
d3	12[mm]	Pump Chamber Diameter
t3	0.5[mm]	Pump Chamber Thickness
d4	1[mm]	Inlet/Outlet Chamber Diameter
t4	0.5[mm]	Inlet/Outlet Chamber Thickness
theta	10[degree]	Nozzle -Diffuser Angle
L	1.5[mm]	Nozzle - Diffuser Length

Table 2. Design parameters for functional layer

The pump chamber diameter (12 mm) is the same as the diaphragm diameter. As for the pump chamber thickness, sizes greater than 0.5 mm will yield only a smaller displacement. The inlet/outlet diameter (1 mm) and thickness (0.5 mm) are selected in such a way that it can incorporate the nozzle/ diffuser design. The nozzle/ diffuser parameters are chosen in such a way that it ensures efficient sniffing of the air.

3.3. Mechanism of Operation

The piezoelectric actuator consists of a piezoelectric layer along with a electrode layer attached on top of the diaphragm. When an electric field is applied to the top of the piezoelectric disc it induces a deformation on membrane [14]. The applied AC (alternating current) voltage across the piezoelectric membrane leads to an actuating force on the membrane. Due to the elastic property of the membrane, it behaves like a spring creating an oscillatory motion [15]. Oscillatory motion creates an outward (supply mode) and inward deflection (pump mode).

In the supply mode, the outward deflection of the membrane as shown in Figure 3.2. causes an increase in the pump chamber volume which decreases the pressure inside the pump chamber. In this mode there is a fluid flow from the inlet to the outlet.

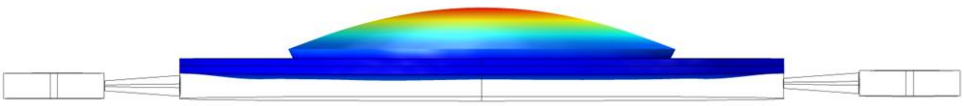

Figure 3. 2 Outward deflection of the membrane in piezoelectric micropump

In the pump mode, the inward deflection of the membrane as shown in Figure 3.3. causes an increase in the pump chamber volume which decreases the pressure inside the pump chamber. In this mode there is a fluid flow from the outlet to the inlet.

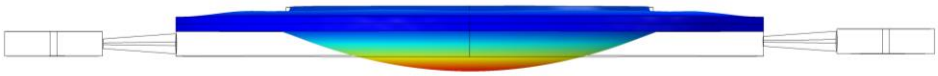

Figure 3. 3 Inward deflection of the membrane in piezoelectric micro[ump

Deviating from the conventional models, this thesis aims to use a DC voltage driven piezoelectric micropump which mimics mammalian olfaction and holds the sniffed air for any desired time while the sensing is still being performed. However in conventional models, the application of AC voltage drives the micropump to pump continuously. With a DC voltage applied, a static deformation and a steady flow rate is achieved. The application of the DC voltage leads to an actuating force on the membrane which drives the flow of the air. The supply mode is achieved by means of a positive voltage whereas the pump mode is achieved by means of a negative voltage. Thus, the pump can mimic the act of sniffing the air in and out.

3.3. Piezoelectric Effect

The piezoelectric effect was discovered by the brothers Pierre and Jacques Curie in 1880 while conducting studies on quartz crystal [36]. Piezoelectricity is the ability of the materials (notably crystals and certain ceramics) to electrically polarize in response to an applied mechanical stress. The polarization is proportional to the applied stress. In inverse piezoelectric effect a mechanical deformation is produced in response to an applied electric field. The inverse piezoelectric effect was predicted by Lippman in 1881 and was confirmed by the Curie brothers [36]. In inverse piezoelectric affect, the application of voltage induces a deformation in the piezoelectric material which generates stress. The stress induced on the diaphragm of the piezoelectric membrane causes the fluid flow. Thus, piezoelectric valveless micropump makes use of the inverse piezoelectric effect to propel the fluid flow [36].

3.3.1. Molecular Model of Piezoelectric Effect

When a material is not subjected to any external stress, the centers of the positive and negative charge of the molecule coincide [36]. As the external effects of the charges are reciprocally cancelled an electrically neutral molecule appears. However, under the application of some external pressure the internal structure of the molecule is deformed. This causes the separation between the positive and negative centers of the molecule generating dipoles. Eventually the facing poles are mutually cancelled. As a result, there is a distribution of linked charge on the material surface and the material becomes polarized. This polarization generates an electric field and can be used to transform the mechanical energy of the material deformation to electrical energy [36].

3.3.2. Constitutive Equations of Piezoelectric Effect

When an external electric field E is subjected to a piezoelectric ceramic medium devoid of mechanical stress, the strain generated is given by [37-38]

$$S = dE \tag{3.1}$$

$$S = gD \tag{3.2}$$

$$S = \frac{d}{\mathcal{E}^T} \tag{3.3}$$

where d, g and $\mathcal{E}^T$ are the material constants. d is the piezoelectric charge constant, g is the piezoelectric voltage constant, $\mathcal{E}^T$ is the permittivity at constant stress and D is the electric displacement respectively.

According to the Hook's law, the strain experienced by an elastic medium subjected to a tensile stress T

$$S = s^E T \tag{3.4}$$

where s^E is the compliance of the medium at a constant electrical field.

The total strain is

$$S = s^E T + dE \tag{3.5}$$

$$S = s^D T + gD \tag{3.6}$$

in which s^E and s^D are respectively the specific compliances at constant electric field and constant electric displacement.

Alternatively, the above equations can be expressed as

$$T = c^E s + eE \tag{3.7}$$

$$D = eS + \mathcal{E}^S T \tag{3.8}$$

Where c^E, e and $\mathcal{E}^S$ are the elasticity at constant electric field, piezoelectric constant at constant mechanical strain and dielectric material constant respectively.

From the theory of bending of plates (in polar coordinates) gives the deflection of a laterally loaded plate.

$$\nabla^4 w = \left(\frac{\partial^2}{\partial r^2} + \frac{1}{r}\frac{\partial}{\partial r} + \frac{1}{r^2}\frac{\partial^2}{\partial \theta^2}\right)\left(\frac{\partial^2 w}{\partial r^2} + \frac{1}{r}\frac{\partial w}{\partial r} + \frac{1}{r^2}\frac{\partial^2 w}{\partial \theta^2}\right) \tag{3.9}$$

$$= \frac{q}{D} \tag{3.10}$$

where w is the lateral displacement, r is the radial distance in polar coordinate, q is the intensity of the lateral load over the plate and D is the flexural rigidity.

The flexural rigidity D is given by the relation

$$D = \frac{Eh^3}{12\,(1 - v^2)} \tag{3.11}$$

where E is the Young's modulus, h is the thickness and v is the Poisson's ratio of the material respectively.

From the lateral displacement obtained, the volume pumped V can be calculated as

$$V = \int_b^a \int_0^{2\pi} wrd\theta dr \tag{3.12}$$

where a is the radius of the membrane and b is the radius of the piezoelectric material.

3.5. Fluid Flow

Piezoelectric valveless micropump involves the coupling of piezoelectricity and fluid flow. On a microscale, a gas is modelled by the kinetic theory, The model assumes that the molecules are very small compared to the relative distance between molecules. The molecules are in constant, random motion and frequently collide with the walls of the enclosed medium. The induced piezoelectric effect by the actuator drives the gas flow. The flow is assumed to be a laminar compressible flow since air is used as the fluid.

3.5.1. Flow Regime

The fluid flow regimes are determined majorly by the Reynold's number and Mach Number.

Reynold's Number (Re) corresponds to the ratio of the inertial forces to the viscous forces [39].

$$Re = \frac{\rho UL}{\mu} \tag{3.13}$$

where ρ, U, L and μ are the density of the fluid, relative speed of the fluid, characteristic length of the system and dynamic viscosity of the fluid respectively.

When Re < 2300, the flow is considered to be laminar [39]. When Re is between 2300 and 4000, the flow is transient whereas when Re > 4000 the flow is turbulent [39].

Flow compressibility is measured by Mach number (M). Mach number is ratio of the fluid velocity (U) to the speed of sound in that fluid (c) [39-40].

$$M = \frac{U}{c} \tag{3.14}$$

When M < 0.3 the flow is incompressible while when the M > 0.3 the flow is compressible.

3.5.2. Navier-Stokes Equation for Fluid Flow

The Navier-Stokes equation governs the motion of the fluid [40]. The equations give a mathematical model of conservation of momentum and conservation of mass of a given fluid.

In order to solve the Navier- Stokes Equation a fluid element is considered. The net force acting on the fluid is mass times the acceleration of the element, which is an application of Newton's second law. Hence, the force $\vec{F}$ acting on the fluid element is given by [39, 41-43]

$$\sum \vec{F} = m\vec{a} \tag{3.15}$$

where m is the mass of the fluid element and $\vec{a}$ is the acceleration the fluid element.

(3.15) can be rewritten as

$$\sum \vec{F} = \rho \frac{Du}{Dt} \tag{3.16}$$

where ρ is the density (mass per unit volume of the fluid) and $\frac{Du}{Dt}$ is the time rate of change of velocity which is $\vec{a}$.

Force acting on the fluid element is the sum of two forces, namely the body force and the surface force. Body force act on the surface of the fluid whereas the surface force acts on the surface of the fluid element. The surface force is due to the pressure and shear and normal stress distribution acting on the surface of the fluid element.

$$\sum \vec{F} = -\nabla \mathrm{p} + \nabla.\tau \tag{3.17}$$

Where ∇ p is the pressure distribution on the surface of the fluid element and $\nabla.\tau$ is the viscous force acting on the fluid element.

The right hand side of (3.15) can be rewritten in substantial derivative form as

$$\rho \frac{Du}{Dt} = \rho \frac{\partial u}{\partial t} + \rho \vec{V}.\nabla u \tag{3.18}$$

Expanding the derivative,

$$\frac{\partial(\rho u)}{\partial t} = \rho \frac{\partial u}{\partial t} + u \frac{\partial u}{\partial t} \tag{3.19}$$

Rearranging,

$$\rho \frac{\partial u}{\partial t} = \frac{\partial(\rho u)}{\partial t} - u \frac{\partial u}{\partial t} \tag{3.20}$$

$$\nabla.\left(\rho\vec{V}u\right) = u\,\nabla.\left(\rho\vec{V}\right) - \left(\rho\vec{V}\right).\nabla\,u \tag{3.21}$$

Substituting (3.20) and (3.22) in (3.18)

$$\left(\rho\vec{V}\right).\nabla\,u = \nabla.\left(\rho\vec{V}u\right) - u\,\nabla.\left(\rho\vec{V}\right) \tag{3.22}$$

(3.23)

$$\rho\frac{Du}{Dt} = \frac{\partial(\rho u)}{\partial t} - u[\frac{\partial(\rho)}{\partial t} + \nabla.(\rho\vec{V}) \; + \nabla.(\rho\vec{V}u)$$

$\frac{\partial(\rho)}{\partial t} + \nabla.(\rho\vec{V})$ is the continuity equation which equals 0.

$$\rho\frac{Du}{Dt} = \frac{\partial(\rho u)}{\partial t} + \nabla.(\rho\vec{V}u) \tag{3.24}$$

From (3.17) and (3.24), we arrive at the conservative form of Navier- Stokes equation.

$$\frac{\partial(\rho u)}{\partial t} + \nabla.\left(\rho\vec{V}u\right) = -\nabla\,\mathrm{p} + \nabla.\tau + \mathrm{F} \tag{3.25}$$

where F is the external force acting on the surface of the fluid.

The Navier-Stokes equation is necessary for modelling and understanding the behavior of compressible fluids like air. Also, the above equations help to understand how the stress induced from piezoelectric actuator is transferred to drive the fluid flow.

The velocity of the piezoelectric micropump at any particular point can be solved by equation 3.16. The actuating force (F) on the piezoelectric membrane causes an oscillatory motion in which the force is transferred to the air as shown in equation 3.25. This transferred force propels the air flow in and out of the chamber mimicking mammalian olfaction.

The Navier-Stokes equation together with the piezoelectric constitutive equations are used to solve the physics of piezoelectric valveless micropump with appropriate boundary conditions for the fluid flow.

3.6. Conclusion

In this chapter, the mechanism of operation of the micropump, piezoelectricity effect, and fluid flow model of the micropump are studied to implement the physics in the finite element analysis software. Furthermore, the constitutive relations of piezoelectricity, the volume of the fluid pumped, and the Navier stokes equation are also studied. However, there are limitations in conducting the analytical model study due to real time errors. Since the investigated micropumps have more layers, the analytical modeling becomes more complex leading to errors. To overcome these limitations and how the design parameters affect the volume of the fluid being pumped, finite element analysis of the micropump is investigated extensively in the next chapter.

CHAPTER 4.

Finite Element Analyses of Piezoelectric Micropump

Piezoelectric micropump is one of the candidates used for e-nose applications. Application of voltage on the piezoelectric layer induces a force which causes the displacement of the membrane to sniff the air in and out. The volume integral of displacement gives the maximum volume that can be pumped out under the pump mode. A finite element analysis for different radii, thickness and shape are studied and investigated in this chapter to obtain the displacement and corresponding volume of the air sniffed out.

4.1. Finite Element Analyses – COMSOL

Finite Element analysis is a numerical approach which uses partial differential equations and associated physics equations to calculate the displacement and the volume of a designed sensor or device. There are several finite element analysis software like Ansys, COMSOL and so on. This thesis makes use of COMSOL Multiphysics platform to calculate the displacement and maximum volume sniffed out by using boundary conditions.

4.2. Boundary Conditions

COMSOL Multiphysics software has an in-built physics section that provides the necessary boundary conditions and solves the equations for a particular application. The proposed model accounts for piezoelectric and fluid structure coupling effects.

Piezoelectric effect solves for solid mechanics and electrostatics modules. For solid mechanics part membrane, edges of the electrode and membrane are assumed to be fixed and are given as the fixed constraint. For electrostatics we choose the piezoelectric layer as the domain. A voltage of is applied to the top of the piezoelectric layer. The bottom of the piezoelectric layer acts as the ground.

Fluid structure interaction solves for laminar flow and solid mechanics. For fluid-structure interaction compressible laminar flow is considered which makes use of naiver-

stokes equation. One of the boundaries of inlet chamber is given as inlet. One of the boundaries of outlet chamber is given as outlet. Except for these two boundaries all others are considered as walls. A no slip boundary condition is added at the walls.

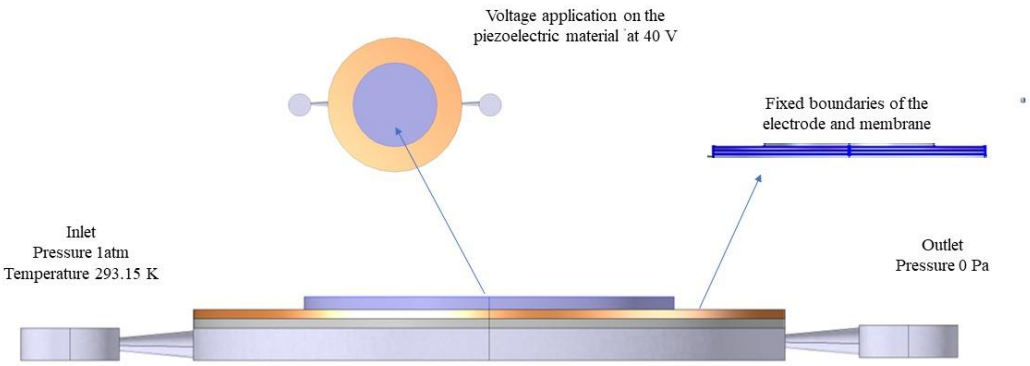

Figure 4. 1 Boundary Conditions applied on the piezoelectric micropump in COMSOL Multiphysics platform

4.3. Meshing

Meshing is a concept in which the device or sensor geometry is divided into tiny domains. In each of these domains the partial differential equations and associated physics equations are applied to arrive at a conclusive result which is independent of the solution. COMSOL offers different types of meshing which includes extra coarser, coarser, coarse, normal, fine, finer, and extra finer.

The adoption of any of the above meshes divides the geometry of the device or sensor into domain which is further subdivided into elements. The extra coarser has lower number of elements whereas the extra finer has the highest number of elements. The meshing with highest density of elements requires more computation time and memory space.

In order to select a suitable mesh, the displacement of the micropump must be independent of the mesh type. Meshing is independent of the solution, as it is a pre-processing step to create a mesh structure that can be used by any numerical method. The

mesh structure defines how the partial differential equations are discretized and how the solution will be approximated.

As observed from Figure 4.2. the displacement becomes independent for coarse mesh biased at 40 V for the design parameters listed in Table 1. In this work a physics fine, extra coarse meshing is applied to minimize computational timing as well as memory space. Also, there is an inaccuracy of 300 nm in the chosen model. For fine mesh, the deflections are in the range of 950 nm. Whereas for extra coarse mesh the deflections are in the range 0f 700 nm.

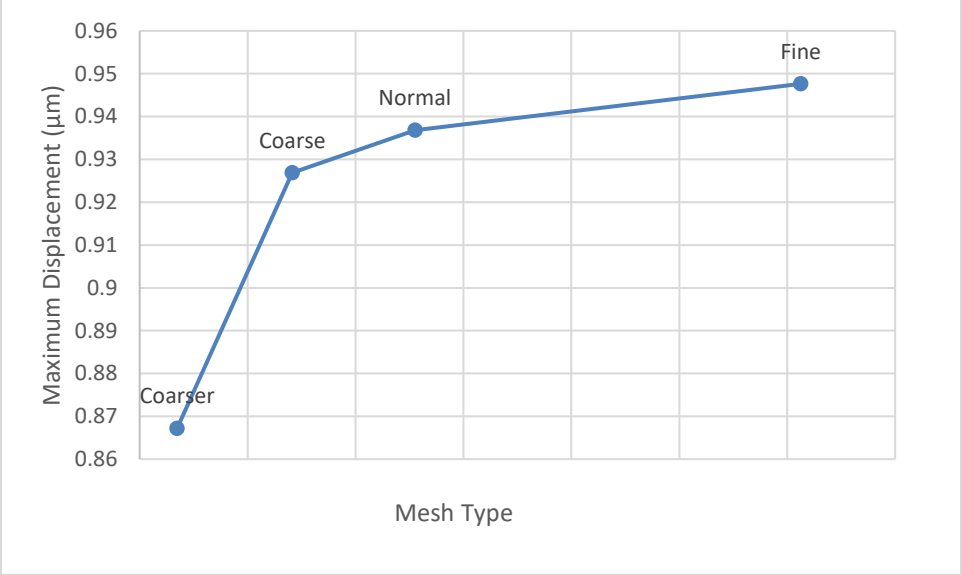

Figure 4. 2. COMSOL Simulation results showing the maximum displacement versus mesh type for a piezoelectric micropump biased at 40 V

4.4. Parametric Analyses on Different Geometries

4.4.1. Effect of PZT layer

For analyzing the effect of the PZT layer, the diameters are chosen in such a way it is less than the diameter of the Cu layer. The following values listed in Table 3. are chosen to study how the increase in the diameter of the piezoelectric layer value affects the maximum displacement and volume as discussed in section 3.2 of Chapter 3. The following values are chosen so as to study how the increasing coverage of the PZT layer on the pump chamber affects the displacement and volume. The thickness of the PZT

layer and Copper layer are chosen for ease of fabrication since sizes less than 0.1 mm are difficult to fabricate. The The PDMS diaphragm diameter and pump diameter are the same since the pump chamber needs to be enclosed. As explained in Chapter 3, the maximum voltage that can be applied to the PZT layer is 160 V. Hence the values chosen for voltage are 40 V, 80 V and 160 V. Herea fine mesh was chosen for studying the effect of the PZT layer diameter and thickness.

When the voltage is applied for the increasing diameter, the force acting on the membrane increases. However there exists a maximum allowable stress for a material, after which force as well as the corresponding displacement reduces. As the diameter of the PZT layer increases the displacement reduces as depicted in the Figure 4.3. The volume follows the similar trend as shown in Figure 4.4 for the parameters listed in Table 3. Figure 4.5 depicts the trend of the stress for various PZT layer diameters. The micropump achieves a maximum allowable stress value at 9.5 mm diameter after which the operation of micropump is critical. Hence the displacement is maximum at the maximum allowable stress value of the micropump.

d	5.5, 7.5, 8, 9.5,11.5, 12[mm]	PZT layer diameter
t0	0.2[mm]	PZT layer thickness
d1	12[mm]	Brass disc external diameter
t1	0.14[mm]	Brass disc thickness
d2	12[mm]	PDMS diaphragm diameter
t2	0.15[mm]	PDMS diaphragm thickness
d3	12[mm]	Pump Chamber diameter
t3	0.5[mm]	Pump Chamber Thickness
Vin	40, 80, 120[V]	Applied Volatge
theta	10[degree]	Nozzle Angle
L	1.5[mm]	Nozzle - Diffuser Length

Table 3. Parameters for studying the effect of PZT layer diameter

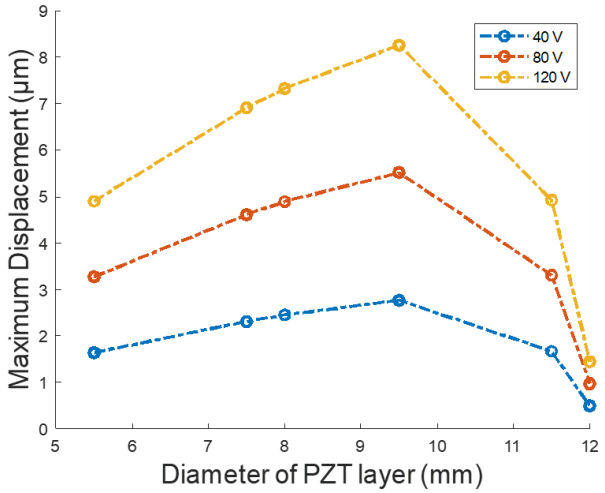

Figure 4. 3. . Maximum displacement for various diameters of PZT layer of the micropump biased at 40 V, 80 V and 120V

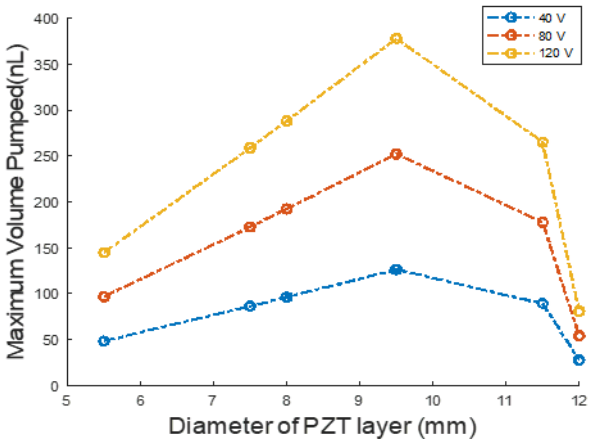

Figure 4. 4. Maximum volume pumped for various diameters of PZT layer of the micropump biased at 40 V, 80 V and 120V

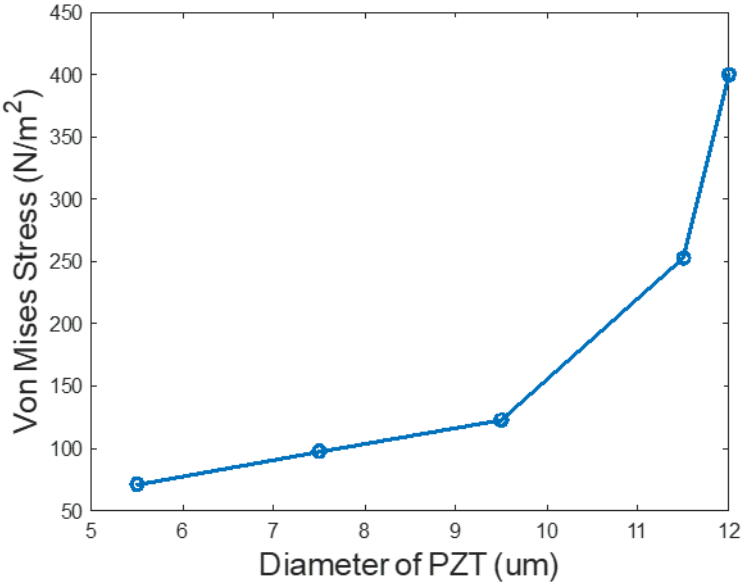

Figure 4. 5. Von Mises Stress for various PZT layer diameters biased at 40 V using COMSOL Multiphysics Platform

For studying the effect of the PZT layer thickness on displacement and volume, sizes greater than 0.1 mm are selected. For values less than 0.1 mm, the process of fabrication becomes difficult. Hence the values of 0.1, 0.2, 0.3 and 0.4 mm. PZT layer thickness follows a different trend from the PZT layer diameter for the following parameters as listed in Table 4. The displacement reduces with increase in the piezoelectric layer thickness. The decrease in displacement is attributed to the flexural rigidity of the material. The flexural rigidity varies with different geometries which causes the decrease in the displacement as well as the volume of air pumped as shown in Figures 4.6. and 4.7.

d	7.5[mm]	PZT layer diameter
t0	0.1, 0.2, 0.3, 0.4[mm]	PZT layer thickness
d1	12[mm]	Brass disc external diameter
t1	0.14[mm]	Brass disc thickness
d2	12[mm]	PDMS diaphragm diameter
t2	0.15[mm]	PDMS diaphragm thickness
d3	12[mm]	Pump Chamber diameter
t3	0.5[mm]	Pump Chamber Thickness
Vin	40, 80, 120[V]	Applied Volatge
theta	10[degree]	Nozzle Angle
L	1.5[mm]	Nozzle - Diffuser Length

Table 4. Parameters for studying the effect of PZT layer thickness

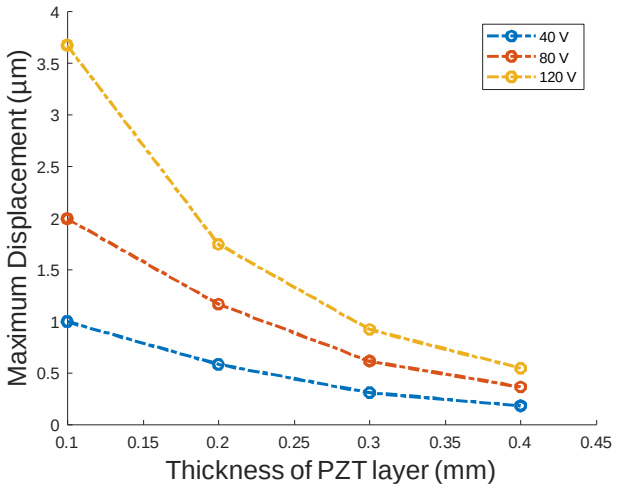

Figure 4. 6. Maximum displacement for various thickness of PZT layer of the micropump biased at 40 V, 80 V and 120V

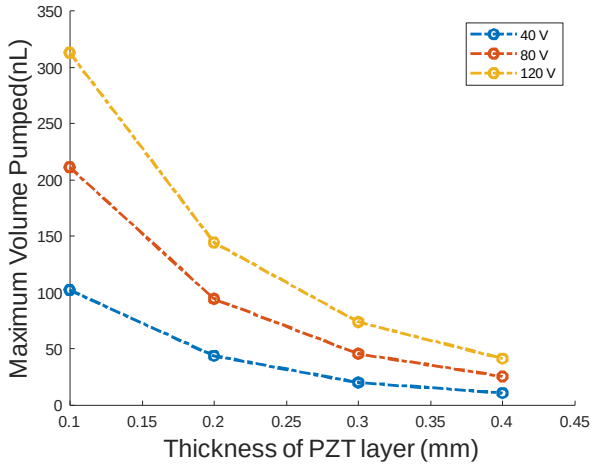

Figure 4. 7. Maximum volume pumped for various thickness of PZT layer of the micropump biased at 40 V, 80 V and 120 V

4.4.2. Effect of PDMS Membrane

For analyzing the effect of the PDMS membrane, both the diaphragm and pump chamber diameter are the same since the pump chamber needs to be enclosed by the membrane layer. The effect of the PDMS membrane thickness on the displacement and volume of air pumped is analyzed using COMSOL software. The thickness values chosen are 0.15 mm, 0.20 mm, 0.25 mm and 0.3 mm. The thickness values less than 0.15 mm are difficult

to fabricate. Hence the values are listed in Table 5 are chosen. Here for reducing the computation time, an extra coarse physics mesh was employed.

When the voltage is applied for the increasing thickness of PDMS membrane the associated bending moment of the PDMS increases. This in turn increases the flexural rigidity of the material which limits the bending strain as shown in Figure 4.7 for the parameters listed in Table 5. The volume of the air pumped is shown in Figure 4.8.

d	7.5[mm]	PZT layer diameter
t0	0.2[mm]	PZT layer thickness
d1	12[mm]	Brass disc external diameter
t1	0.14[mm]	Brass disc thickness
d2	12[mm]	PDMS diaphragm diameter
t2	0.15, 0.20, 0.25, 0.30[mm]	PDMS diaphragm thickness
d3	12[mm]	Pump Chamber diameter
t3	0.5[mm]	Pump Chamber Thickness
Vin	40 [V]	Applied Volatge
theta	10[degree]	Nozzle Angle
L	1.5[mm]	Nozzle - Diffuser Length

Table 5. Parameters for studying the effect of PZT layer thickness

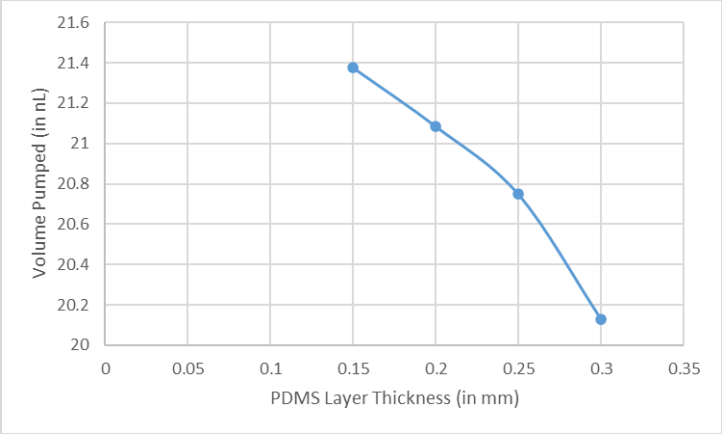

Figure 4. 8. Maximum displacement for various thickness of PDMS layer of the micropump biased at 40 V

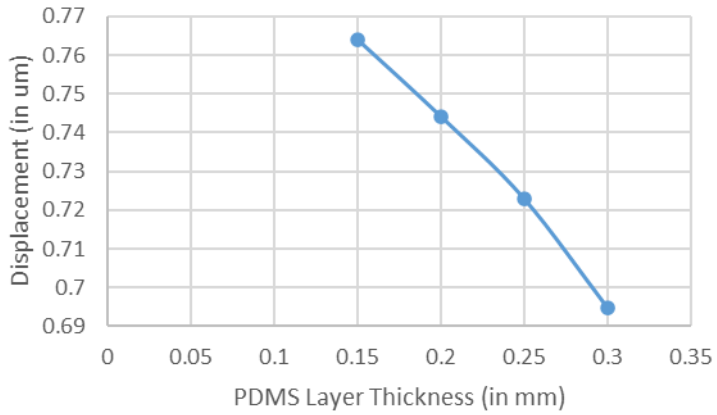

Figure 4. 9. Maximum volume pumped for various thickness of PDMS layer of the micropump biased at 40 V

4.4.3. Effect of Pump Chamber

As explained in 4.4.2. the diameter values are the same for pump chamber and PDMS membrane. The effect of the pump chamber thickness on the diameter and the volume of the air pumped is analyzed. The pump chamber thickness of sizes greater 0.1 mm are chosen in order to overcome the difficulty in fabrication for smaller sizes. The chosen thickness values are 0.2 mm, 0.3 mm, 0.4 mm and 0.5 mm. Here for reducing the computation time, an extra coarse physics mesh was employed.

As the pump chamber height is varied as listed in Table 6, due to the application of voltage, the air molecules compress inside the pump chamber. This builds up a pressure which reduces the bending strain of the membrane as shown in Figure 4.10. It is observed that the displacement drops and then again increases. The rise in the displacement and volume is because the pressure again reduces inside the pump chamber, hence the volume increase. The increase in the displacement is because the pressure required to move larger volume of the fluid is less compared to the pressure which is required for moving shorter volume of the fluid at the previous thickness of the pump chamber. When the thickness of the pump chamber is further increased, the volume of the air required to fill the pump chamber becomes too large for the piezoelectric material to displace effectively. Hence, the displacement decreases. As a result, the pressure required to pump air exceeds the capabilities of the piezoelectric material. The volume of the air pumped follows the

bending strain as shown in Figure 4.11. The result obtained from COMSOL Multiphysics shows that the change in both displacement and volume is negligible.

d	7.5[mm]	PZT layer diameter
t0	0.2[mm]	PZT layer thickness
d1	12[mm]	Brass disc external diameter
t1	0.14[mm]	Brass disc thickness
d2	12[mm]	PDMS diaphragm diameter
t2	0.15[mm]	PDMS diaphragm thickness
d3	12[mm]	Pump Chamber diameter
t3	0.2, 0.3, 0.4, 0.5[mm]	Pump Chamber Thickness
Vin	40 [V]	Applied Volatge
theta	10[degree]	Nozzle Angle
L	1.5[mm]	Nozzle - Diffuser Length

Table 6. Parameters for studying the effect of pump chamber thickness

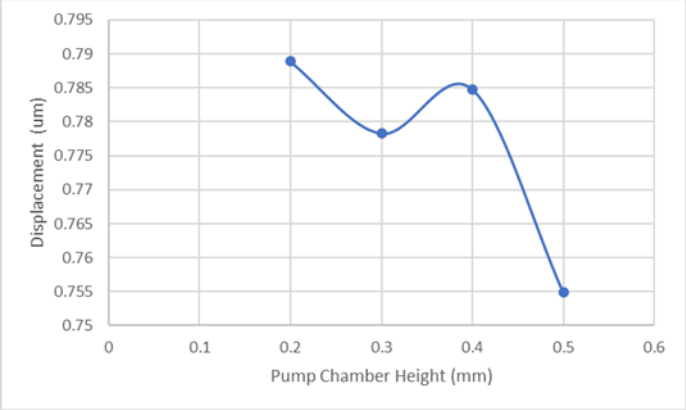

Figure 4. 10. Maximum displacement for various thickness of pump chamber of the micropump biased at 40 V

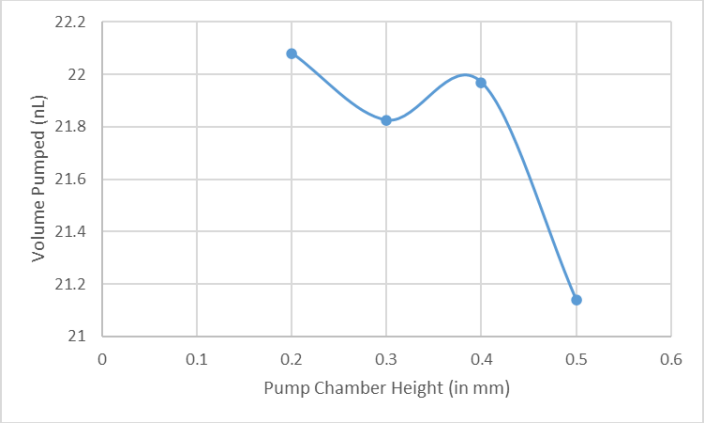

Figure 4. 11. Maximum volume pumped for various thickness of pump chamber of the micropump biased at 40 V

4.4.4. Effect of Nozzle-Diffuser Elements

A conical micro-diffuser/nozzle consists of an inlet and exit as shown in Figure 4.12. Here L refers to the length of the conical diffuser or nozzle. Along with this inlet and exit radius (R1 and R2) of the conical diffuser or nozzle, the half angle of the cone θ is calculated.

$$\theta = tan^{-1}\left(\frac{R1-R2}{L}\right) \tag{4.1}$$

For analyzing the effects of nozzle-diffuser elements, the angle and length of the elements are taken into consideration. According to professor A H Gibson, flow separation occurs for values greater than 15 degrees. Hence the angles are varied from 5, 7, 9, 11 and 13 degrees. When voltage is applied to the piezoelectric layer, the change in the membrane causes a pressure drop in the nozzle-diffuser elements. As a result, the air is pumped in and out of the chamber. The pressure drops decrease both the displacement as well as the volume pumped decreases as shown in Figures 4.13. and 4.14 as the angle of the elements is increased for the parameters listed in Table 4.7. As the nozzle angle is increased, the flow resistance of the nozzle eventually starts to decrease, which reduces the pressure drop across the nozzle. This lower pressure drop then causes a decrease in

the displacement of the piezoelectric actuator, as less energy is required to overcome the lower resistance to flow.

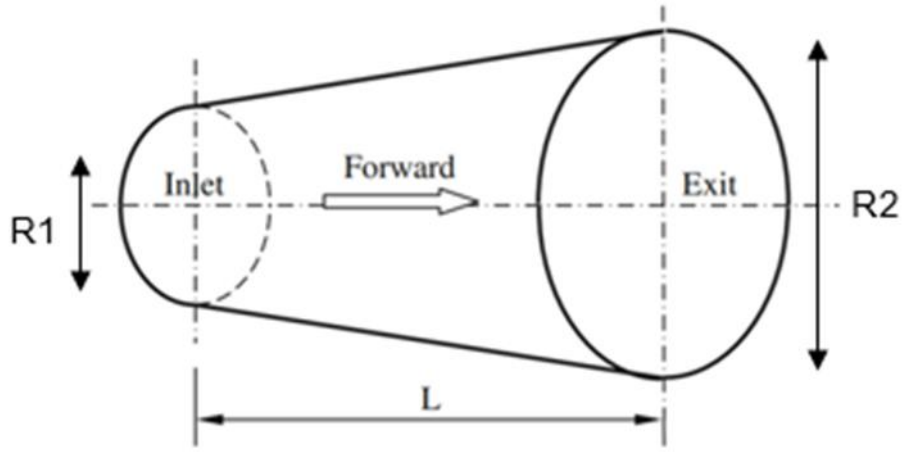

Figure 4. 12. Schematic diagram of a Conical Nozzle- Diffuser

d	7.5[mm]	PZT layer diameter
t0	0.2[mm]	PZT layer thickness
d1	12[mm]	Brass disc external diameter
t1	0.14[mm]	Brass disc thickness
d2	12[mm]	PDMS diaphragm diameter
t2	0.15[mm]	PDMS diaphragm thickness
d3	12[mm]	Pump Chamber diameter
t3	0.5[mm]	Pump Chamber Thickness
Vin	40 [V]	Applied Volatge
theta	5, 7, 9, 10, 11,13[degree]	Nozzle Angle
L	1.5[mm]	Nozzle - Diffuser Length

Table 7. Parameters for studying the effect of nozzle-diffuser angle

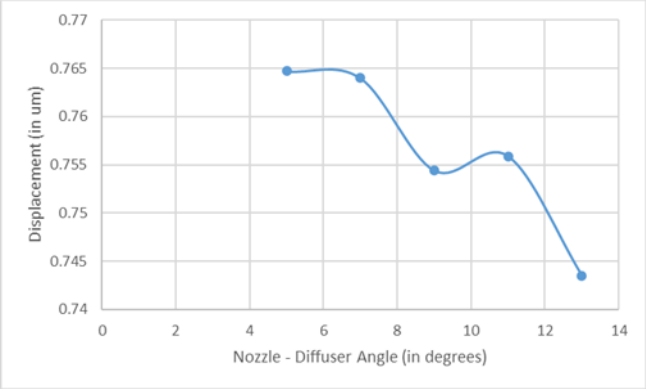

Figure 4. 13. Maximum displacement for various nozzle-diffuser angles biased at 40 V

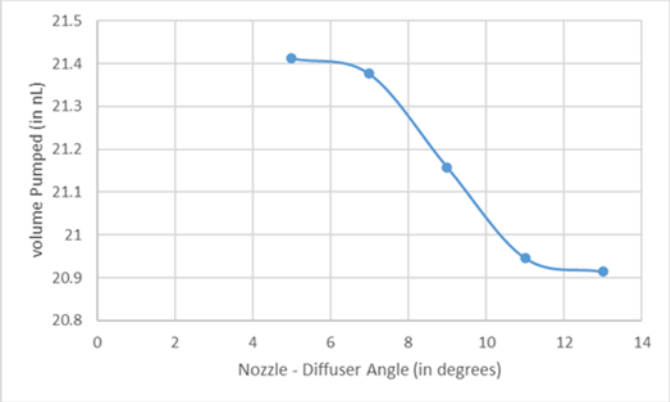

Figure 4. 14. Maximum volume pumped for various nozzle-diffuser angles biased at 40 V

For analyzing the effects of the nozzle-diffuser length, the parameter values chosen are 0.5, 1, 1.5 and 2 mm in order to maintain a nozzle-diffuser angle of 7 degree for which the previous study indicated a good displacement. When the nozzle length is increased, the flow resistance of the nozzle initially increases, which causes a higher pressure drop across the nozzle. This higher pressure drop increases the displacement of the piezoelectric actuator, as more energy is required to overcome the higher resistance to flow. However, as the nozzle length is increased further, the flow resistance of the nozzle eventually starts to decrease, which reduces the pressure drop across the nozzle. This lower pressure drop then causes a decrease in the displacement of the piezoelectric actuator, as less energy is required to overcome the lower resistance to flow.

Moreover, the increase in nozzle length may also lead to a reduction in the fluid velocity at the nozzle outlet, as the fluid has to travel a longer distance to exit the nozzle. This decrease in fluid velocity may also result in a decrease in actuator displacement.

The investigational analysis showed that the voltage applied reduces the pressure across the nozzle-diffuser elements. For values greater than 2 mm the pressure drop will be higher. Hence the following parameters were chosen. As the length of the conical nozzle-diffuser increases, both the displacement as well as the volume pumped increases and then decreases as shown in Figures 4.15 and 4.16 for the parameters listed in Table 8.

d	7.5[mm]	PZT layer diameter
t0	0.2[mm]	PZT layer thickness
d1	12[mm]	Brass disc external diameter
t1	0.14[mm]	Brass disc thickness
d2	12[mm]	PDMS diaphragm diameter
t2	0.15[mm]	PDMS diaphragm thickness
d3	12[mm]	Pump Chamber diameter
t3	0.5[mm]	Pump Chamber Thickness
Vin	40 [V]	Applied Volatge
theta	7[degree]	Nozzle Angle
L	0.5, 1, 1.5, 2[mm]	Nozzle - Diffuser Length

Table 8. Parameters for studying the effect of nozzle-diffuser length

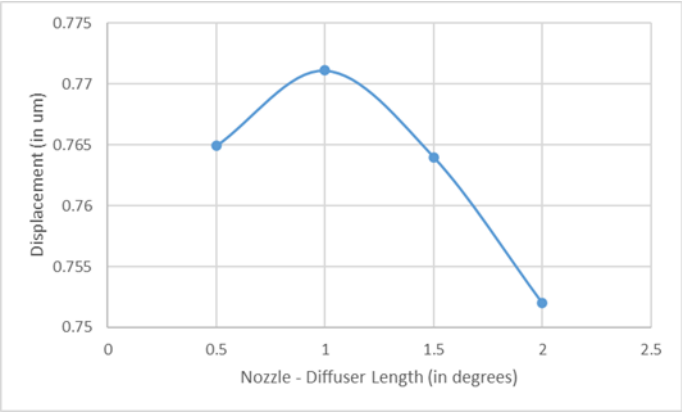

Figure 4. 15. Maximum displacement for various nozzle-diffuser lengths biased at 40 V

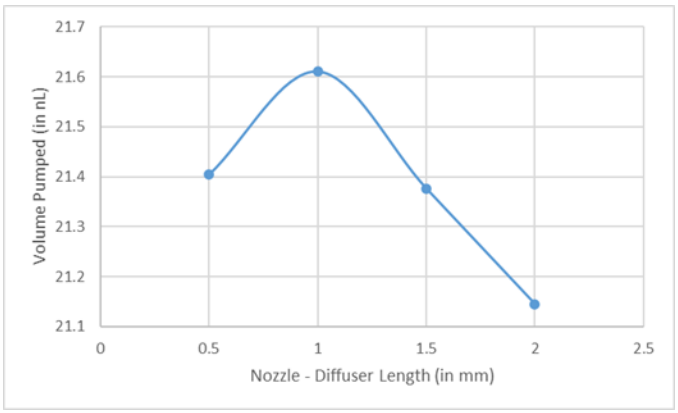

Figure 4. 16. Maximum volume pumped for various nozzle-diffuser lengths biased at 40 V

4.5. Conclusion

In this chapter a finite element analysis is conducted for analyzing the effect of different critical parameters. The critical design parameters such as diameters, thickness, angles and lengths are studied. The boundary conditions are discussed along with the appropriate physics. From the studied parameters it was obtained that there was a negligible change in displacement and volume pumped for the nozzle-diffuser designs. However, other parameters such as radii and thickness of the electrode layers provides results that can be used for the fabrication of the sensor.

CHAPTER 5

Conclusion and Future Scope

The odor of the plants can be sniffed in using an e-nose mechanism to effectively detect the pest control problems during asymptotic stages. Hence the crops can be protected, and the pest can be eradicated. Deviating from the conventional approach of volatile organic compound detection using mass spectroscopy, the e-nose system considers an array of sensors and pattern recognition algorithm to detect volatile organic compounds.

The e-nose system uses the micropump mechanism to effectively sniff the volatile organic compounds produced by the plants. Thus, the micropump can mimic mammalian olfaction. The advantages of using the micropump include faster response time and better displacement. Compared to the conventional bulky approaches, miniaturization is an added advantage of the proposed system.

In this work, a piezoelectric micropump which can mimic mammalian olfaction with the application of DC voltage model was designed by conducting a comprehensive review on all the available micropumps which is able to sniff in and out air for a smaller time period. Based on the literature review between mechanical and non-mechanical micropumps, piezoelectric based micropump was chosen as the candidate for mimicking mammalian olfaction.

The working mechanism and governing equations for the piezoelectrically actuated model was investigated. The critical parameters were identified. The inverse piezoelectric effect and fluid mechanics governing the model were investigated. Based on the investigation a piezoelectric effect based micropump which can mimic mammalian olfaction was studied using the computational platform COMSOL Multiphysics.

Computational analysis was carried out using COMSOL Multiphysics platform where the effect of the critical parameters were studied. Mesh studies were conducted using COMSOL Multiphysics. The effect of the PZT layer indicated that a diameter of 9.5 mm and a thickness of 0.1 mm offered better displacement as well as volume pumped. The

effect of the PDMS membrane analyses concluded that a small thickness owed to better displacement and volume. The effect of the pump chamber analyses conducted gave a negligible change in displacement and volume due to the varying pressure drops. The effect of the nozzle-diffuser elements also showed a similar trend as the effect of the pump chamber. The change in the displacement and volume associated with the change in the angle and length of nozzle-diffuser elements were small.

5.1. Future Scope

The proposed model designed in the finite element analysis platform COMSOL required more computational time for achieving the results. Several studies were previously conducted in order to achieve the mimicking capability before choosing the application of DC voltage to achieve the results. Hence the studies conducted on the model were limited.

More parametric sweeps can be performed by varying the different membrane materials such as polymeric and ceramic diaphragm materials. Also, various other actuator geometries can be incorporated to study its effect on displacement as well as the volume of the air being pumped. A detailed fabrication method needs to be implemented for the proposed design.

REFERENCES/BIBLIOGRAPHY

[1]. G. LaPlante *et al.*, “Canadian Greenhouse Operations and Their Potential to Enhance Domestic Food Security,” *Agronomy*, vol. 11, no. 6, p. 1229, Jun. 2021, doi: 10.3390/agronomy11061229.

[2]. M. López-Gresa et al., "A New Role for Green Leaf Volatile Esters in Tomato Stomatal Defense Against Pseudomonas syringe pv. tomato", *Frontiers in Plant Science*, vol. 9, p. 1855, 2018. Available: 10.3389/fpls.2018.01855.

[3]. M. Richter, “Microdosing 58. Microdosing of Scents,” p.1-18.

[4]. A. Nisar, N. Afzulpurkar, B. Mahaisavariya, and A. Tuantranont, “MEMS-based micropumps in drug delivery and biomedical applications,” *Sensors and Actuators B: Chemical*, vol. 130, no. 2, pp. 917–942, Mar. 2008, doi: 10.1016/j.snb.2007.10.064.

[5]. Liguo Chen, Yaxin Liu, Lining Sun, Dongsheng Qu and Jijiang Min, "Intelligent control of Piezoelectric Micropump based on MEMS flow sensor," *2010 IEEE/RSJ International Conference on Intelligent Robots and Systems*, Taipei, 2010, pp. 3055-3060, doi: 10.1109/IROS.2010.5649844.

[6]. A. Nisar, N. Afzulpurkar, B. Mahaisavariya, and A. Tuantranont, “MEMS-based micropumps in drug delivery and biomedical applications,” *Sensors and Actuators B: Chemical*, vol. 130, no. 2, pp. 917–942, Mar. 2008.

[7] .R. Zengerle, A. Richter, and H. Sandmaier, “A micro membrane pump with electrostatic actuation,” in *[1992] Proceedings IEEE Micro Electro Mechanical Systems*, Travemunde, Germany, 1992, pp. 19–24.

[8]. J. W. Judy, T. Tamagawa, and D. L. Polla, “Surface-machined micromechanical membrane pump,” in *[1991] Proceedings. IEEE Micro Electro Mechanical Systems*, Nara, Japan, 1991, pp. 182–186.

[9]. C. Cabuz, W. R. Herb, E. I. Cabuz, and Son Thai Lu, “The dual diaphragm pump,” in *Technical Digest. MEMS 2001. 14th IEEE International Conference on Micro Electro Mechanical Systems (Cat. No.01CH37090),* Interlaken, Switzerland, 2001, pp. 519–522.

[10]. T. Bourouina, A. Bossebuf, and J.-P. Grandchamp, “Design and simulation of an electrostatic micropump for drug-delivery applications,” *J. Micromech. Microeng.*, vol. 7, no. 3, pp. 186–188, Sep. 1997.

[11]. H.T.G. Van Lintel, F.C.M. van De Pol, S. Bouwstra, A piezoelectric micropump based on micromachining of silicon, Sens. Actuators. 15 (2) (1988) 153–167.

[12]. M. Koch, N. Harris, A.G.R. Evans, N.M. White, A. Brunnschweiler, A novel micromachined pump based on thick film piezoelectric actuation, Sens. Actuators A: Phys. 70 (1998) 98–103.

[13]. C.G.J. Schabmueller, M. Koch, M.E. Mokhtari, A.G.R. Evans, A. Brunnschweiler, H. Sehr, Self-aligning gas/liquid micropump, J. Micromech. Microeng. 12 (2002) 420–424.

[14]. K. Junwu, Y. Zhigang, P. Taijiang, C. Guangming, W. Boda, Design and test of a high performance piezoelectric micropump for drug delivery, Sens. Actuators A: Phys. 121 (2005) 156–161.

[15]. S.W. Lee,W.Y. Sim, S.S. Yang, Fabrication and invitro test of a microsyringe, Sens. Actuators A: Phys. 83 (2000) 17–23.

[16]. G.H. Feng, E.S. Kim, Piezoelectrically actuated dome-shaped diaphragm micropump, J. Microelectromech. Syst. 14 (2005) 192–199.

[17]. A. Geipel, A. Doll, F. Goldschmidtboing, P. Jantscheff, N. Esser,U. Massing, P.Woias, Pressure independent micropump with piezoelectric valves for low flow drug delivery systems,MEMS2006, Istanbul, Turkey, 22–26 January, 2006.

[18] . B. Ma, L. Sheng, Z. Gan, G. Liu, X. Cai, H. Zhang, Z. Yang, A PZT insulin pump integrated with a silicon micro needle array for transdermal drug delivery, in:

Proceedings of the *56th Electronic Components and Technology Conference*, 2006, pp. 677–681.

[19]. O. C. Jeong and S. S. Yang, “Fabrication and test of a thermopneumatic micropump with a corrugated p+ diaphragm,” *Sensors and Actuators A: Physical*, vol. 83, no. 1–3, pp. 249–255, May 2000.

[20]. S. Zimmermann, J. A. Frank, D. Liepmann, and A. P. Pisano, “A planar micropump utilizing thermopneumatic actuation and in-plane flap valves,” in *17th IEEE International Conference on Micro Electro Mechanical Systems. Maastricht MEMS 2004 Technical Digest*, Maastricht, Netherlands, 2004, pp. 462–465.

[21]. F. C. M. Van de Pol, H. T. G. Van Lintel, M. Elwenspoek, and J. H. J. Fluitman, “A thermopneumatic micropump based on micro-engineering techniques,” *Sensors and Actuators A: Physical*, vol. 21, no. 1–3, pp. 198–202, Feb. 1990, doi: 10.1016/0924-4247(90)85038-6.

[22]. W.L. Benard, H. Kahn, A.H. Heuer, M.A. Huff, “A titanium–nickel shape memory alloy actuated micropump,” in: *International Conference on Solid State Sensors and Actuators*, vol. 1, 1997, pp. 361–364.

[23]. D. Xu, L. Wang, G. Ding, Y. Zhou, A. Yu, and B. Cai, “Characteristics and fabrication of NiTi/Si diaphragm micropump,” *Sensors and Actuators A: Physical*, vol. 93, no. 1, pp. 87–92, Aug. 2001.

[24]. G. Shuxiang, T. Fukuda, “SMA actuator based novel type of micropump for biomedical application”, in*: IEEE International Conference*, vol. 2, 2004, pp. 1616–1621.

[25]. S. Guo, K. Asaka, “Polymer based new type of micropump for biomedical applications”, in: Proceedings of the *IEEE Conference on Robotics & Automation Taipei,* Taiwan, 2003, pp. 1830–1835.

[26]. W.Y. Sim, H.J. Yoon, O.C. Jeong, S.S. Yang, “A phase change type of micropump with aluminum flap valves”, *J. Micromech. Microeng*. 13(2003) 286–294.

[27]. R. Boden, M. Lehto, U. Simu, G. Thornell, K. Hjort, J.A. Schweitz, “A polymeric paraffin micropump with active valves for high pressure microfluidics”, in: Proceedings of the *13th International Conference on Solid State Sensors, Actuators and Microsystems,* Seoul, Korea, 2005, pp. 201–204.

[28]. K.S. Yun, I.J. Cho, J.U. Bu, C.J. Kim, E. Yoon, “A surface tension driven micropump for low voltage and low power operations”, J. MEMS l.11(2002) 454–461.

[29]. J.H. Tsai, L. Lin, “A thermal bubble actuated micro nozzle-diffuser pump,microelectromechanical systems”, in: Proceedings of the *14th IEEE International Conference,* 2001, pp. 409–412.

[30]. J.D. Zahn, A. Deshmukh, A.P. Pisano, D. Liepmann, “Continuous onchip micropumping for microneedle enhanced drug delivery”, Biomed.Microdev. 6 (2004) 183–190.

[31]. H. Suzuki, R.Yoneyama, “Areversible electrochemical nanosyringe pump and some considerations to realize low power consumption”, Sens. Actuators B: Chem. 86 (2002) 242–250.

[32]. Y. Yoshimi, K. Shinoda, M. Mishima, K. Nakao, K. Munekane, “Development of an artificial synapse using an electrochemical micropump”, J. Artif. Organs 7 (2004) 210–215.

[33]. A. Kabata, H. Suzuki, “Microsystem for injection of insulin and monitoring of glucose concentration”, in: Proceedings of the *5th International conference on Sensors,* Sensors 2005, 2005, pp. 171–174.

[34]. C.S. Effenhauser,H. Harttig, P. Kramer, “An evaporation-based disposable micropump concept for continuous monitoring applications”, Biomed.Microdev. 4 (1) (2002) 27–33.

[35]. D. Japikse, N. C. Baines, and D. Japikse, *Diffuser design technology*. Norwich, VT: Concepts ETI, 1995.

[36] W. Heywang, K. Lubitz, and W. Wersing, Eds., *Piezoelectricity: Evolution and Future of a Technology*. Berlin Heidelberg: Springer-Verlag, 2008. doi: 10.1007/978-3-540-68683-5.

[37] F. E. H. Tay, "Design Rules for Micropumps," *Microfluidics and BioMEMS Applications*, pp. 25–51, 2002, doi: 10.1007/978-1-4757-3534-5_2.

[38] H. Asadi Dereshgi, H. Dal, and M. Z. Yildiz, "Piezoelectric micropumps: state of the art review," *Microsyst Technol*, Jan. 2021, doi: 10.1007/s00542-020-05190-0.

[39] F. M. White, *Fluid Mechanics*. McGraw Hill, 2011.

[40] "What Are the Navier-Stokes Equations?" https://www.comsol.com/multiphysics/navier-stokes-equations (accessed Sep. 27, 2021).

[41] S. Schneiderbauer and M. Krieger, 'What do the Navier- Stokes Equations mean ?', vol. 015020, doi: 10.1088/0143-0807/35/1/015020.

[42] John D Anderson, 'Computational Fluid Dynamics: Chapter 2: Governing Equations of Fluid Dynamics', Comput. Fluid Dyn., pp. 15–51, 2009, [Online]. Available: http://link.springer.com/10.1007/978-3-540-85056-4.

[43] M. Raju, "Design of a Regulated Micromachined Air-Sniffer Using Thermal Transpiration Effect for E-Nose Applications," *Electronic Theses and Dissertations*, Jun. 2021, [Online]. Available: https://scholar.uwindsor.ca/etd/8612

VITA AUCTORIS

NAME:	Yameema Babu Lopez
PLACE OF BIRTH:	Kerala, India
YEAR OF BIRTH:	1996
EDUCATION:	Alphonsa English Medium School, Kerala, India, 2015
	APJ Abdul Kalam Technological University, B.Tech., Kerala, India, 2019
	University of Windsor, M.Sc., Windsor, ON, 2023